8 Properties of a Polarized Light-Beam Multiply Scattered by a Rayleigh Medium

K.I. Hopcraft[1], P.C.Y. Chang[2], J.G. Walker[2], and E. Jakeman[1]

[1] School of Mathematical Sciences, Theoretical Mechanics Division
[2] School of Electrical and Electronic Engineering,
University of Nottingham,
Nottingham
NG7 2RD
UK

Abstract. Multiple scattering of an incoherent beam of polarized light propagating through a random medium is studied using Monte-Carlo simulations. The medium comprises a slab of monodispersive spherical Rayleigh particles. Spatial, angular and path-length distributions of the scattered light are examined in both transmission and backscatter. The change of polarization state is discussed as a function of propagation distance for two initial states. Contrasting linear with circularly polarized light shows the former to be better preserved in all the results obtained. Backscattered light is dominated by single scattering events occurring from the medium closest to the exit plane.

1 Introduction

Multiple scattering of radiation has been the subject of many investigations over the last 50 or so years [1]-[23] being motivated by a desire to understand the behaviour of light passing through or scattering from an inhomogeneous atmosphere. There have been many theoretical attempts to solve the problem, the first of which was a continuum theory where the transport of energy was key. This radiative transfer theory [2,3] has proved difficult to solve for all but the simplest cases, such as plane wave propagation through plane-parallel atmospheres, hence other methods have been devised. These range from the 'small angle approximation', where the direction of a ray after scattering is a perturbation of its direction prior to scattering, to diffusion theory, where the direction of a ray after scattering is isotropically distributed [4]. More recent work on beam propagation includes calculations of the impulse shape using the diffusion approximation and show its dependence on the width of a Gaussian profile beam [5].

The temporal spread of backscattered radiation was examined experimentally and theoretically using linearly polarized light [6]. It was shown that light returning to a detector earliest has its initial polarization state largely intact, whilst at later times the light becomes depolarized. In [7] was noted sinusoidal azimuthal variations in the co- and cross-polar intensities for

F. Moreno and F. González (Eds.): Lectures 1998, LNP 534, pp. 135−158, 2000.

when the equation of radiative transfer was solved for a plane wave propagating at normal incidence to a slab comprising spherical particles. Angular lineshape calculations were studied in [8, and references therein] for coherent backscatter in the regime of weak localization and found qualitative agreement with experimental results, and similarly [9] found good agreement with experiments for angular lineshapes in both transmission and reflection using a much simplified multiple scattering theory. In the topic of diffusing-wave spectroscopy [10], the way in which the polarization state is affected by propagation through random media and differences between the behaviour of linearly and circularly polarized light has been addressed. This was further commented upon in [11] in the context of entropy production.

The purely analytic work has been restricted to the limits of multiple scattering where the number of scattering events is very low or very high. The entire range of light scattering can however, be explored with numerical simulations. One class of computer simulations is known as the 'Monte-Carlo' method [26,27] which is a stochastic approach to problem solving. This is particularly useful in the study of incoherent light scattering as it simulates the flow of energy through a medium.

This paper provides results from a classical Monte-Carlo simulation of vector light scattering for the purpose of investigating the behaviour of polarized light as it propagates through a medium. The adjective 'classical' refers to the simulation being a one-to-one analogue of the physical process. Non-classical simulations are ones in which variance reduction techniques have been introduced to accelerate the statistical convergence of results [15,19]. Monte-Carlo simulations have been used many times in the past for unpolarized light [12–15], but fewer workers have analysed polarized light, see however [16–23]. Most of these simulations have been written for specific applications from lidar evaluations, through visibility studies, to astrophysical simulations. This paper sets out to rigorously examine the polarization properties of multiply scattered light in its entirety. Whilst a few aspects have been touched upon by the aforementioned work, those simulations were tied to particular configurations of detection such as small field of view and measuring exclusively in transmission or backscatter using linearly or circularly polarized light. This paper examines the cases of linear and circular initial polarization states extensively with all permutations of output variables (including exit positions, exit angles and path lengths) and their influence on final polarization states. The differences in behaviour of linear and circular polarization reported in [10] have, in part, prompted this study to examine the possibility of exploiting the use of polarization information as a discriminant for imaging and detection in scattering media.

There are two ways to incorporate polarization information into a Monte-Carlo simulation: by using Stokes vectors with the full scattering matrix [16,17,19–23] or using a simple helicity state [18]. Here the former method is used as the latter treats circularly polarized light alone. It should be stres-

sed that, with notable exceptions [16,21,23], few previous simulations have implemented polarization effects rigorously. The simulation described here explores some of the more fundamental aspects of the vector multiple scattering problem.

The spherical scatterers are assumed to be small enough for the Rayleigh approximation to apply [24]. Among the past simulations, other scattering models for the medium, such as an ensemble of Mie scatterers [24] (describing exactly spherical particles of arbitrary size) and the heuristic Henyey-Greenstein model [25] have been used, see [16,17,20,21,23] and [15,18,19,22] for respective examples of such usage.

The results presented have a variety of applications, including: studying the transfer of solar radiation through clouds [12]; simulating backscattering/transmission of laser light from/through clouds [13,17]; studying visibility in foggy conditions [14]; examining image formation through turbid media [15]; establishing whether polarized light can discriminate short-path photons [18]; studying polarized pulse propagation through turbid media [19]; determining the influence of particle size on the depolarization of light [20]; simulating polarization maps of light emissions from protostellar dust envelopes [21,22]; and to simulate light emissions from dusty spiral galaxies [23].

In the next section, the structure of the Monte-Carlo code is described together with an explanation for how the direction of a light ray and its polarization state changes upon scattering from a particle. Section 3 defines the quantities measured from the simulation data, such as the degree of polarization and shows the results of such measurements. Further diagnostics derived from the data are obtained in Sect. 4, which shows the dependence of the degree of polarization and other quantities on exit position, exit angles and propagation path-length. Section 5 provides a summary and conclusion. The appendix gives details for how the polarization state relates to the scattering geometry and derives the phase function for the scattering angles.

2 Description of Model

This section outlines a Monte-Carlo simulation for describing the characteristics of polarized radiation that exactly models the scattering events caused by small (sub-wavelength sized) spherical particles. It predicts the final destination of multiply scattered rays by launching a beam from the origin that propagates parallel to the z-axis in the first instance, as depicted in Fig. 1.

The instantaneous polarization state of each ray is carried along its journey by the simulation. The scattering medium occupies the semi-infinite half-space $z > 0$ and comprises an ensemble of Rayleigh scatterers distributed randomly throughout the medium.

The Monte-Carlo simulation requires three elements to model the scattering. These determine:

- when and where an individual scattering event occurs

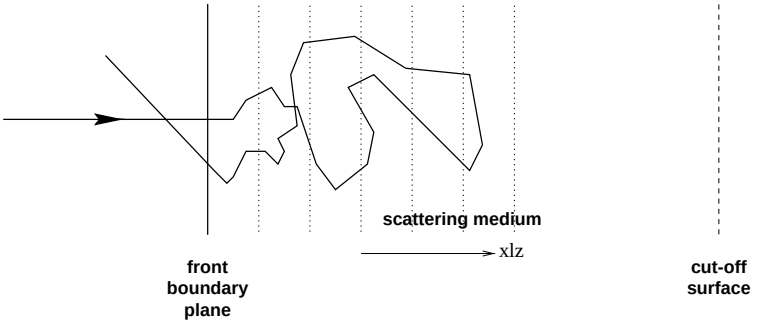

Fig. 1. An illustration of the simulation geometry

- how the interaction with a particle alters both the trajectory and subsequent polarization state of a ray
- how the local coordinate system carried by a ray changes after a scattering event.

In addressing the first element it is assumed that scattering medium is isotropic and homogeneous, hence the probability density for the distance s travelled by a ray before it encounters a particle is determined by a negative exponential distribution with a given mean free path characterizing the size (or length scale) of the medium. Altering the size of the mean free path would make the medium more, or less dense but is here set to unity to define a scale length. A given ray propagates a random distance s drawn from the distribution before encountering a particle. The particle then scatters the ray, changing its direction of propagation and polarization state. The state of the ray is described in terms of the Stokes vector [2,24],

$$\mathbf{S} = (I, Q, U, V)\,. \tag{1}$$

The first component I represents the intensity of the ray. In the calculations presented this component is assigned a value of unity, *i.e.* as if scattering from a particle and the propagation between particles are both lossless. Q is the difference between the intensities of two orthogonal polarization components resolved at angles of 0 and $\pi/2$ relative to a reference axis in the plane perpendicular to the ray direction. U is a similar measure with polarization components resolved at $\pi/4$ and $3\pi/4$ in the same plane. V is the difference in intensity between right and left circularly polarized components.

The second element of the simulation concerns the trajectory and polarization state of a ray subsequent to a scattering event. This requires knowledge of the scattering amplitudes of the particles comprising the medium. For Rayleigh scatterers the angular part of the intensity distribution of the scattered light, usually referred to as the 'phase function', adopts the simple

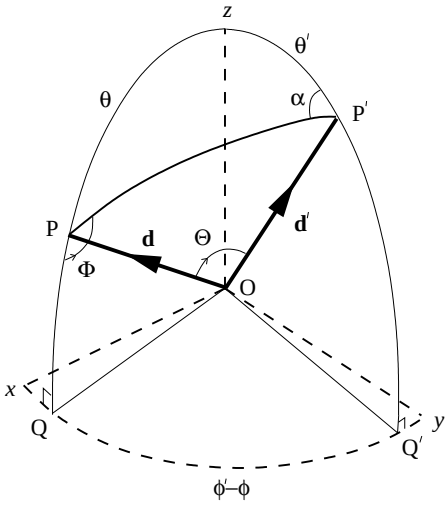

Fig. 2. The scattering geometry of the ray directions

analytical form

$$P(\mu, \Phi, \mathbf{S}) = \frac{3}{16\pi} \left[\left(\mu^2 + 1\right) + \left(\mu^2 - 1\right) \left(Q \cos 2\Phi + U \sin 2\Phi\right) \right] , \qquad (2)$$

where $\mu = \cos \Theta$, Θ is the scattering angle between the incoming and outgoing ray directions and Φ is the azimuthal angle through which the ray is rotated (see Fig. 2). This phase function acts as a joint probability density function for determining the direction in which the ray propagates following its encounter with the particle and depends upon the polarization state of the impinging ray. In Fig. 3 the polar surface plots show the phase function for linear and circular polarized light. The linear phase function is not axisymmetric about the incident light direction due to the Φ dependence of (2). The circular phase function is axisymmetric because the incoming light has no Q or U components. The linear phase function is broader in the y direction and has a null point in the x direction. It is also important to note the forward/backward symmetry of the scattered intensity arising because of the small particle size.

The scattered intensities in particular polarization states are calculated in the appendix and the results are depicted in Figs. 4 and 5. The co-polarized component shown on the left of Fig. 4 has larger magnitude than the cross-polar component shown on the right. The cross-polar component has several null points, two of which are in the direct forward and back-scattered directions. This is also the case for circularly polarized light as shown in Fig. 5, the right-forward component is much larger than left-forward component. The mirror symmetry between right and left components stems from the convention of using helicity as a reference. The backward left component rotates

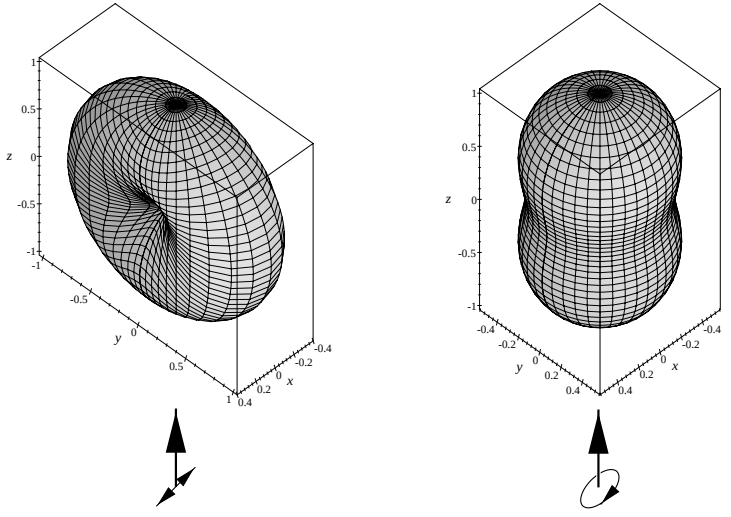

Fig. 3. Polar plots of the phase function for scattering from Rayleigh particles. The left figure shows the linearly polarized case and the right is for circularly polarized light. The incident light propagates in the positive z direction and scatters from a particle situated at the origin. The linearly polarized light is initially polarized in the x direction. The large arrows show the incident direction and the small arrows indicate the initial polarization state

in the same sense as the forward right component but their propagation directions are opposite. The fraction of light scattered into the other polarization state can be calculated from (16) to (21) in the appendix. For linearly polarized light, this fraction is 1/16 and for circular polarization it is 1/8. So from each scattering it is apparent that circularly polarized light is twice as likely to be scattered into its opposite state as linearly polarized light.

The scatter angles for determining the direction of a ray are generated using the inversion and rejection methods on the marginal and conditional probabilities derived from the phase function [27,28]. Of the published polarization simulations mentioned in the introduction, only two use non-uniform distributions for Φ [21,23]. The other simulations [17–20,22] use the uniform distribution for Φ which is a questionable simplification due to the dependence of the phase function on the incoming polarization state and Φ in (2) and the form that these take as shown in Fig. 3.

The new Stokes vector $\mathbf{S}'$ that results from the scattering interaction is easily determined through the Mueller matrix $\mathbf{M}$ which, in this instance [24]

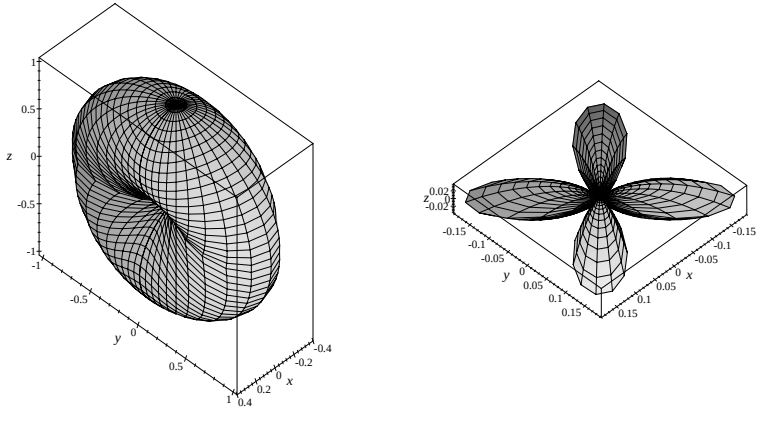

Fig. 4. Polar plots of single-scattering intensities for linear input. The left figure shows the co-polarized component and the right is for cross-polarized light

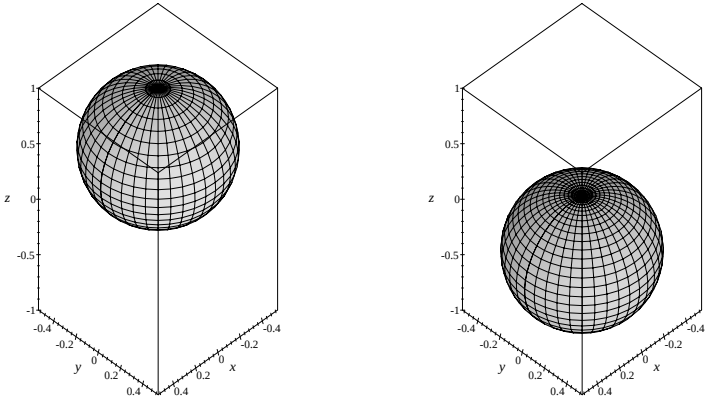

Fig. 5. Polar plots of single-scattering intensities for circular input. The left figure shows the right-circularly polarized component and the right figure is for left-circularly polarized light

is a simple function of the scattering angle Θ

$$\mathbf{M}(\mu) = \frac{1}{2}\begin{pmatrix} \mu^2+1 & \mu^2-1 & 0 & 0 \\ \mu^2-1 & \mu^2+1 & 0 & 0 \\ 0 & 0 & 2\mu & 0 \\ 0 & 0 & 0 & 2\mu \end{pmatrix}. \tag{3}$$

The final element of the simulation determines the local coordinate transformation that is required following the scattering event. This transformation defines the plane in which the polarization vector lies along with the direction of the reference axis. The new Stokes vector $\mathbf{S}'$ is obtained from the old Stokes vector $\mathbf{S}$ using

$$\mathbf{S}' = \mathbf{T}(-\alpha)\mathbf{M}(\mu)\mathbf{T}(\Phi)\mathbf{S} \tag{4}$$

where $\mathbf{T}$ is the rotation matrix

$$\mathbf{T}(\alpha) = \begin{pmatrix} 1 & 0 & 0 & 0 \\ 0 & \cos 2\alpha & \sin 2\alpha & 0 \\ 0 & -\sin 2\alpha & \cos 2\alpha & 0 \\ 0 & 0 & 0 & 1 \end{pmatrix}, \tag{5}$$

and α is the angle labelled in Fig. 2.

There is a finite probability that a few rays may meander in a lateral direction within the slab and consequently may travel a long distance before emerging from the exit plane. Introducing a hemispherical boundary of predetermined size (taken to have a radius of sixty mean free paths in the simulations that follow) limits the extent of the scattering domain and also the high computational overhead that entails following such errant rays. Hence any ray that traverses this boundary is effectively absorbed.

Figure 6 shows the logical steps for the simulation. Each ray carries with it a set of variables describing its state, these are:

- the position of the ray head $\mathbf{r}$
- the direction of the ray $\mathbf{d}$
- the polarization state $\mathbf{S}$
- the total distance travelled by the ray s_t
- the maximum depth penetrated by the ray into the medium $z_{\max}$
- the number of scattering events experienced by the ray N_{scat}.

The four main stages to the simulation [26,3,1] are:

1. a specific initial polarization state is assigned which is then propagated to its first randomly situated scattering site
2. the scattering angles are generated using the phase function (2) and the new polarization state is obtained using (4)

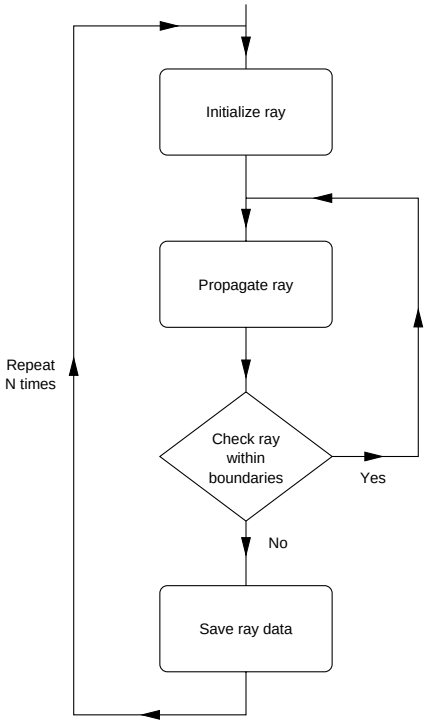

Fig. 6. Flow of Monte-Carlo simulation

3. tests are performed to ascertain whether a ray has passed any relevant surfaces, such as the exit plane, cut-off hemisphere or some other plane used for diagnostic purposes
4. upon traversing a surface, the state of the ray (as listed in the description above) is calculated for the point of interception with the surface. If the surface is the exit plane, the ray is recorded. If the surface is the cut-off hemisphere, the ray is abandoned. In all other cases the ray's state is recorded before it continues its journey by returning to stage 2.

Once the ray has left the scattering domain or has been abandoned, the process is repeated a further $N - 1$ times, where N is sufficiently large to ensure reliable statistics of the derived state variables. Further details of the scattering geometry and the way that the local coordinate system transforms are contained in the appendix. Pseudo-random numbers are generated using the routine `ran2` from [29]. This was selected because it has a very large period of 2×10^{18} guaranteeing that the same sequence of random numbers is not used during a simulation of $N \sim 10^6$ rays.

3 Simulation Results and Discussion

To generate data to study the behaviour of the polarization state of multiply scattered light, the simulation program described in the previous section was run for 2 million rays. All length measures are in units of mean free paths. Two initial polarization states are studied: linear with $\mathbf{S} = (1, 1, 0, 0)$ and right circular with $\mathbf{S} = (1, 0, 0, 1)$.

During the simulated propagation of each ray the first crossing of each of thirty internal boundaries is logged and the response of a virtual detector positioned at each of these planes can be calculated. The response of a particular type of detection system is found for each ray by forming the scalar product of the ray Stokes vector with $\mathbf{S}_i$ describing the detection system. For a detector with no polarization discrimination $\mathbf{S}_i = (1, 0, 0, 0)$, a detector with a linear polarizer in the same orientation as the linearly polarized illumination (co-polar) has $\mathbf{S}_i = (1, 1, 0, 0)/2$, a detector with a linear polarizer in the orthogonal orientation (cross-polar) has $\mathbf{S}_i = (1, -1, 0, 0)/2$, a detector with a circular polarizer in the same orientation as the right-circularly polarized illumination has $\mathbf{S}_i = (1, 0, 0, 1)/2$ and for a detector with a left circular polarizer has $\mathbf{S}_i = (1, 0, 0, -1)/2$.

The degree of polarization (DOP) D quantifies the change in polarization of the scattered rays is defined by

$$D_l = \frac{|I_{\text{co}} - I_{\text{cross}}|}{I_{\text{co}} + I_{\text{cross}}} \tag{6}$$

for linear polarization and by,

$$D_c = \frac{|I_{\text{right}} - I_{\text{left}}|}{I_{\text{right}} + I_{\text{left}}} \tag{7}$$

for circular polarization.

In all plots presented the left vertical scale relates to the intensity and the right vertical scale to the degree of polarization of a particular state. Figure 7 shows the intensity and degrees of polarization that would be detected in transmission through slabs of varying thickness by a spatially-integrating detector.

The transmitted intensity decays from an initial value of unity to 0.053 at a depth $z = 30$. It decreases in a sub-exponential manner as the logarithmic plot in Fig. 8 shows. In fact the intensity has an asymptotic power law dependence with exponent -0.955. The unscattered remainder is governed by an exponential decay. The linear and circular values of D both decay much quicker than the transmitted intensity and beyond $z = 6$ they are less than 0.1. The ratios for linear states always lie above those for the circular states. The jaggedness of the lines in Fig. 8 shows the effect of noise caused by statistical fluctations in our finite sampling. This noise ultimately limits accuracy.

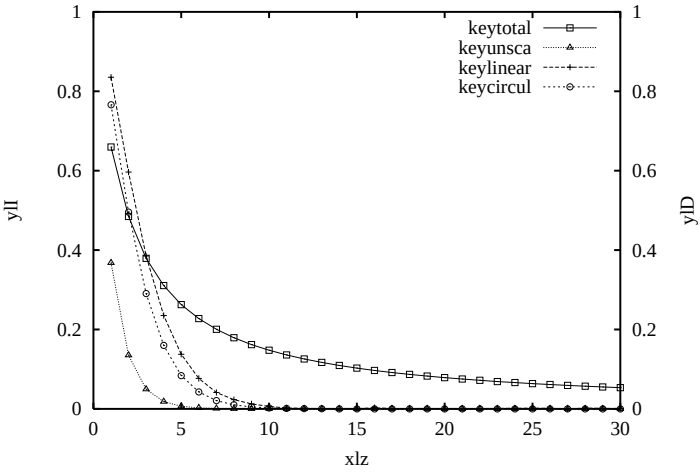

Fig. 7. The transmitted intensity and degree of polarization as a function of slab thickness for linear and circular input polarizations. The left hand vertical scale corresponds to the intensity curve (valid for both linear and circular illumination) and the vertical scale on the right is for linear and circular degrees of polarization. The slab thickness is in units of mean free paths

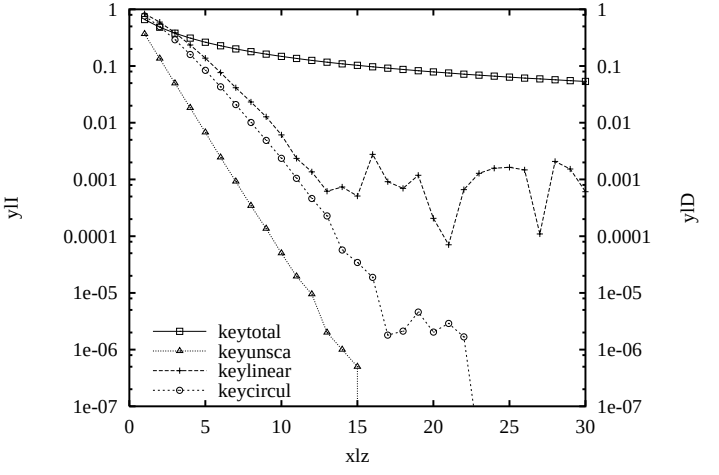

Fig. 8. A log plot of transmitted intensity and degree of polarization against slab thickness for linear and circular input polarizations

Any initial polarization state is scrambled upon the light having reached a depth of about 6 mean free paths. This is equivalent to a ray having experienced (on average) just over 24 scatterings, which is in accord with the figure quoted in [6].

The propagation characteristics of linear polarized light is a little more resilient to depolarization than is circular light. This is in agreement with earlier experimental [10], theoretical [11] and simulation [20] work. The difference in polarization 'memory' was first discussed in [10] and has been attributed to the helicity inversion that circularly polarized light suffers due to the scatterer acting as an optical mirror [10,11,20]. This inversion does not occur for linear polarization so that state is better preserved. A similar line of reasoning leads to the opposite effect occurring for particles whose size is greater than the wavelength of the light. The circular state has greater immunity to depolarization on scattering than does the linear state. This happens since these particles scatter more in the forward direction than Rayleigh particles and so there is less helicity inversion. However the calculations of the previous section indicate that for small particles the difference in behaviour stems from fundamental differences at the single scattering events where the initial polarization state is twice as likely to be changed for circularly polarized light.

The third graph, Fig. 9, shows rays that are backscattered from media of various thicknesses. This is derived from the data by removing contributions from rays that have travelled past a hypothetical absorbent plane located at various depths. The backscattered intensity increases as the medium becomes

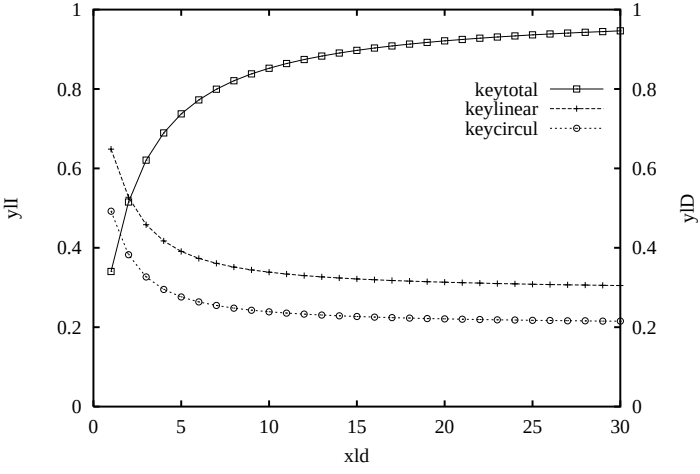

Fig. 9. A plot of backscattered intensity and degree of polarization against slab thickness for linear and circular input polarizations

thicker because rays have a greater chance to scatter back to the input plane. It should increase to unity for an infinitely thick slab, but our hemispherical cut-off surface limits the maximum value to about 0.975 since approximately 2.5% of rays are abandoned after breaching the hemisphere. The linear degree

of polarization decreases from unity to 0.31 whilst the circular ratio declines further to 0.22. This shows that the backscattered light retains some of the original polarization, with the linear input better preserved for the same reasons as those detailed above.

4 Spatial, Angular, and Path-Length Histograms

Whenever a ray intercepts either the exit or an internal reference plane, its state is recorded as described in Sect. 2. In this section, the dependences of the intensity and the degree of polarization with position, direction and the length of path traversed are examined. The distributions of transmitted and backscattered intensities together with those for the degree of polarization are shown as a function of the radial distance from the original axis of propagation to show the degree of beam spreading, and with polar angle to indicate the direction of the ray. Also shown is the azimuthal dependence of these quantities about this axis and the distribution of path-lengths.

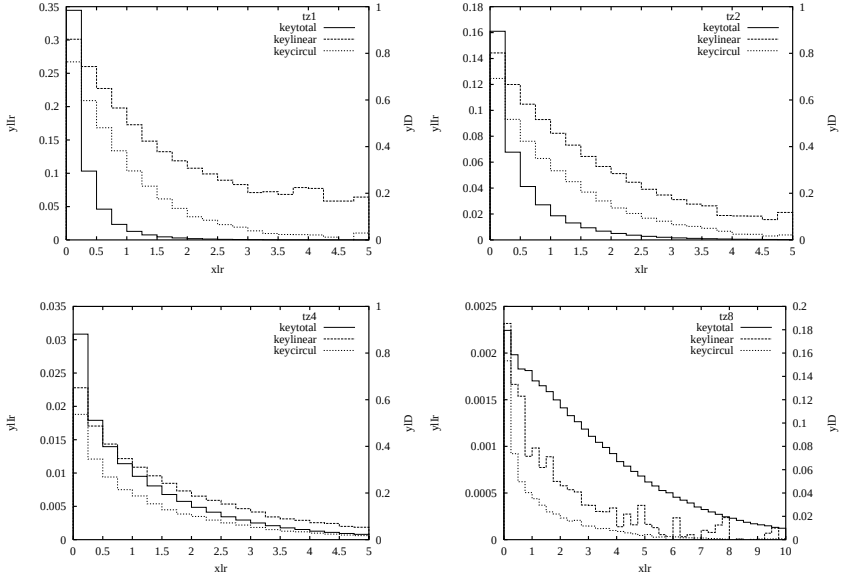

Fig. 10. Transmitted intensity per unit area as a function of radius from the z-axis at depths of $z = 1, 2, 4, 8$.

In Figs. 10 & 11 the point of intersection that each ray makes with a reference plane is binned as a function of the radial distance ρ from the z-axis. The bin size is 0.25 mean free paths wide and the intensity has been scaled by the reciprocal of the midpoint radius of each bin to counter the

bias due to differing bin areas that occurs in a cylindrical-polar coordinate system. In the forward direction, only scattered rays are included in the ensemble. Unscattered rays propagate along the z-axis and therefore have a delta-function distribution at $\rho = 0$ which is not shown.

From Fig. 10 it can be seen the intensities decrease in an approximately exponential manner for sufficiently large values of ρ, hence the beam broadens as it propagates forward. Near to the axis there is a predominance of single scattered light which has retained its polarization state and so the degree of polarization is close to unity. This feature is maintained with increasing depth into the medium. The linear degree of polarization is greater for all radial positions and depths than the circular DOP. This is consistent with the spatial form of the single scattering intensity distributions shown in figures 4 and 5. The graphs for backscattered rays in Fig. 11 are constructed for

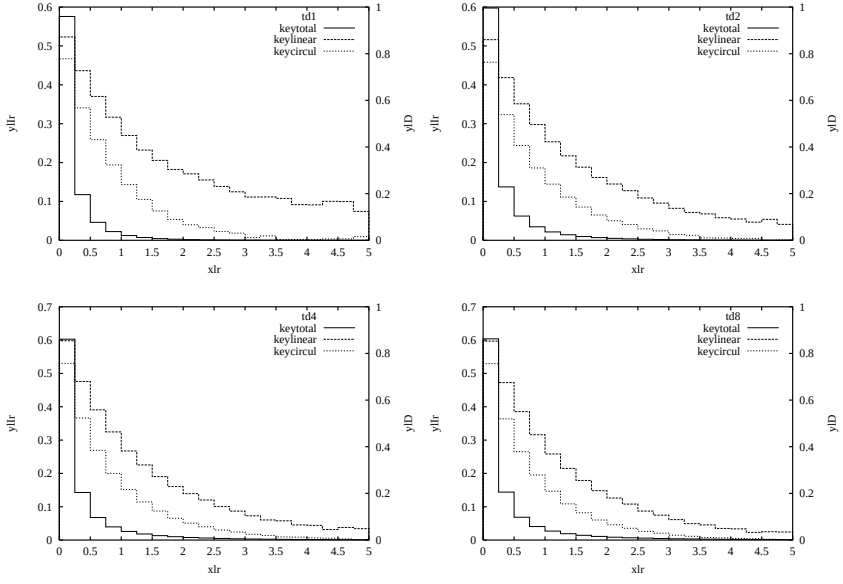

Fig. 11. Backscattered intensity per unit area as a function of radius ρ from the z-axis. An absorbing screen is positioned at distances $z = 1, 2, 4, 8$

hypothetical absorbing screens positioned at distances $z = 1, 2, 4, 8$ mean free paths, thus simulating the effect of slabs having different thicknesses. These show little qualitative difference in the behaviour of the DOPs from those shown for the transmitted rays that reach a depth of one mean free path, thus demonstrating the fore-aft symmetry of Rayleigh scatterers. The results are insensitive to the slab thickness, showing that the backscattered results

are dominated by single scattering events from the immediate surrounding medium.

The polar angle distribution of the exit rays is plotted in Figs. 12 & 13. Here, $\theta = 0°$ corresponds to the forward propagating direction and $\theta = 90°$ propagation perpendicular to the z-axis. The bin widths are 5° and the intensity is normalized by the sine of the angle between the z-axis and each bin's midpoint.

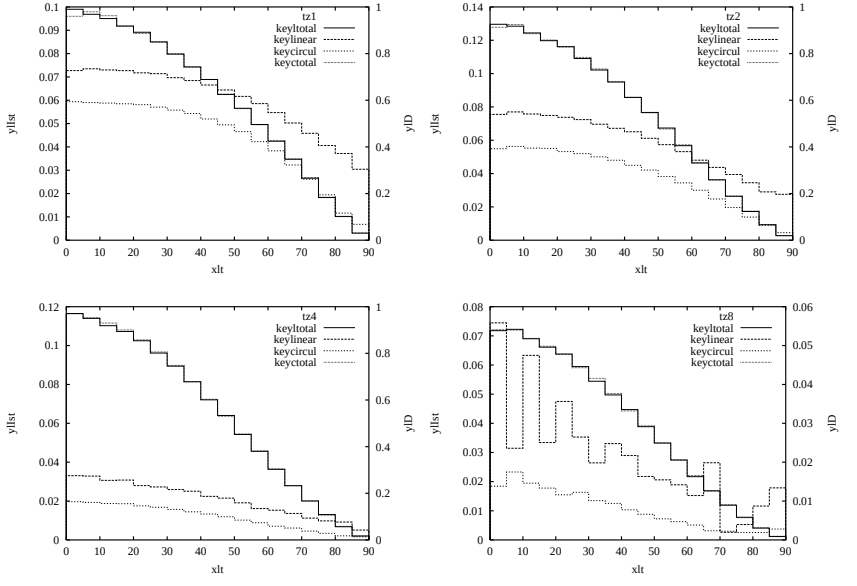

Fig. 12. Plots of transmitted intensity per unit solid angle against polar angle at depths of $z = 1, 2, 4, 8$. Only the contributions from scattered rays are shown.

Again, only the scattered rays are considered. The unscattered rays have a delta-function distribution in the forward scattering direction $\theta = 0°$. In Figs. 12 & 13 the DOP curves have similar behaviour to each other, though again the linear polarization is greater than circular polarization. By 8 mean free paths into the medium the polarization is no longer angle dependent and all memory of the initial polarization state has been erased.

The distribution of the rays with azimuthal angle is shown in Figs. 14 & 15. The bins are 10° wide. As before, only scattered rays are shown. In the forward direction at $z = 1$ the intensity curve for linear polarization varies sinusoidally with angle ϕ. This due to the variation of the linearly polarized intensity as depicted in Fig. 4. This strong variation with ϕ is smoothed out with increasing propagation into the medium. Note also that the circular

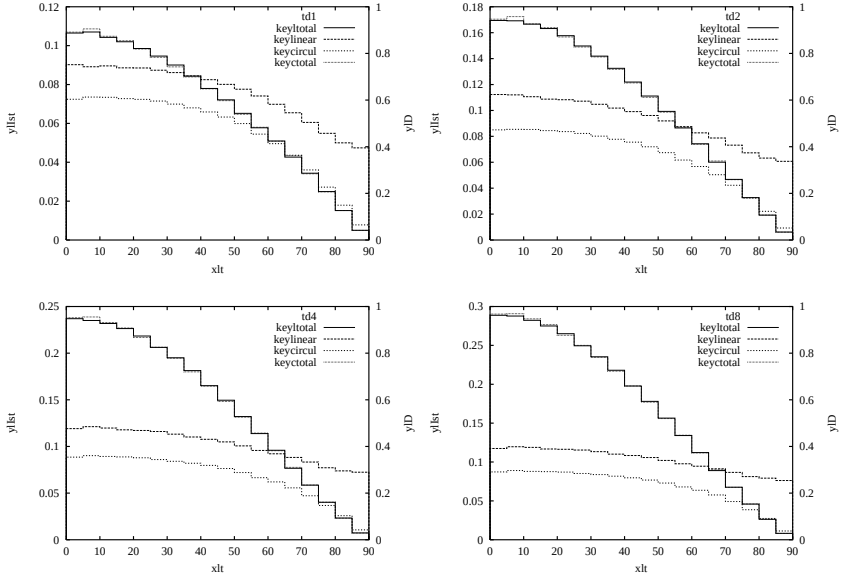

Fig. 13. Plots of backscattered intensity per unit solid angle as a function of polar angle for slab thicknesses $z = 1, 2, 4, 8$

polarization state is initially isotropic with ϕ and hence remains so with increasing propagation distance.

The distributions for backscattered rays are shown in Fig. 15 for progressively thicker slabs. These exhibit a similar asymmetry in azimuthal distribution of the linear polarization state for the same reasons as given before. However the distributions are not smoothed out in this instance because of the dominant effect of single scattering events in the backscattered direction. The general behaviour of the intensity distributions with ϕ is similar to that found in [7] where the radiative transfer equation was solved numerically. This provides some credence for using continuum models to describe scattering behaviour from ensembles of discrete entities.

Finally the logarithm of the distribution of the intensity as a function of the total path-length s_t traversed by rays before they exit the medium is shown in Figs. 16 & 17. The bin width is 0.5 mean free path. Note in Fig. 16 that the decay of the intensity is exponential for depths up to $z = 4$, beyond which a second maximum appears away from $s_t = z$. The second maxima indicate that the rays follow a most likely path length. This may be interpreted as the path length for which multiple scattering is most likely to occur since the inter-scatter propagation rule for single scattering no longer applies. The DOP curves confirm this view as they indicate that most of the initial polarization information has been eradicated at large depths into the medium. The tails of these curves also have an exponential distribution. Note

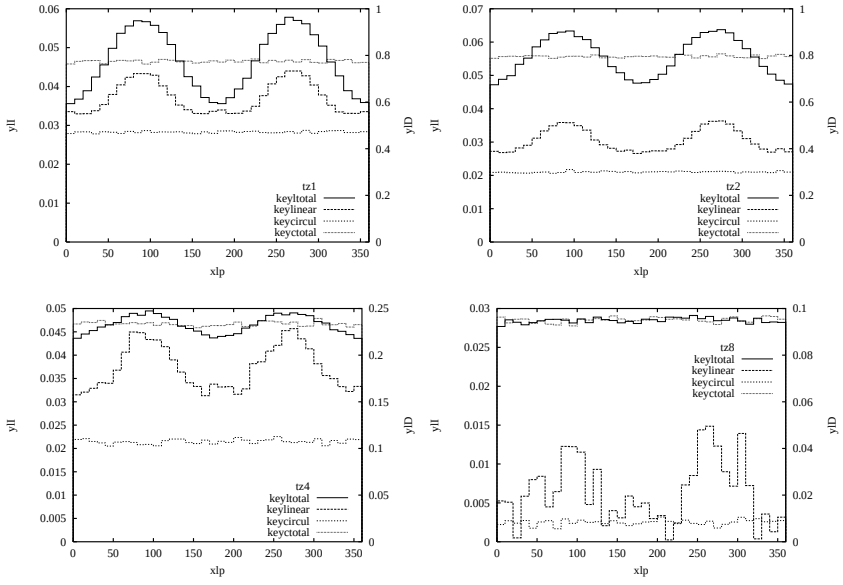

Fig. 14. Plots of transmitted intensity per unit solid angle against azimuthal angle at depths of $z = 1, 2, 4, 8$. Only the contributions from scattered rays are shown.

that the proportion of ballistic rays ($s_t = z$) decline with increasing depth into the medium, to the extent that there are almost none at a depth of $z = 8$.

The logarithm of the backscattered intensity as a function of path-length is shown in Fig. 17. For thin slabs, the distribution has an exponential tail. For thicker slabs ($z \geq 4$) the backscattered intensity follows a power law at long path lengths with exponent -1.117. The DOP curves decay away for longer path-lengths which shows that the rays that travel further are (obviously) scattered more times.

5 Summary and Conclusions

This paper has examined the way in which a beam of radiation has its state of polarization altered upon propagation through a random medium comprising an ensemble of spherical Rayleigh particles. The scattering phase functions particular to these particles are treated exactly and multiple scattering effects are modelled by tracing the destination and polarization state of a bundle of rays using a Monte-Carlo simulation. The scattering medium has a slab geometry and its optical density can be changed by altering the mean free path of a ray between successive particle encounters. Various measures can be constructed from the simulation data that may be replicated under experimental conditions. This aspect of the present work has not been comprehensively addressed in previous treatments of polarization effects in multiple scattering

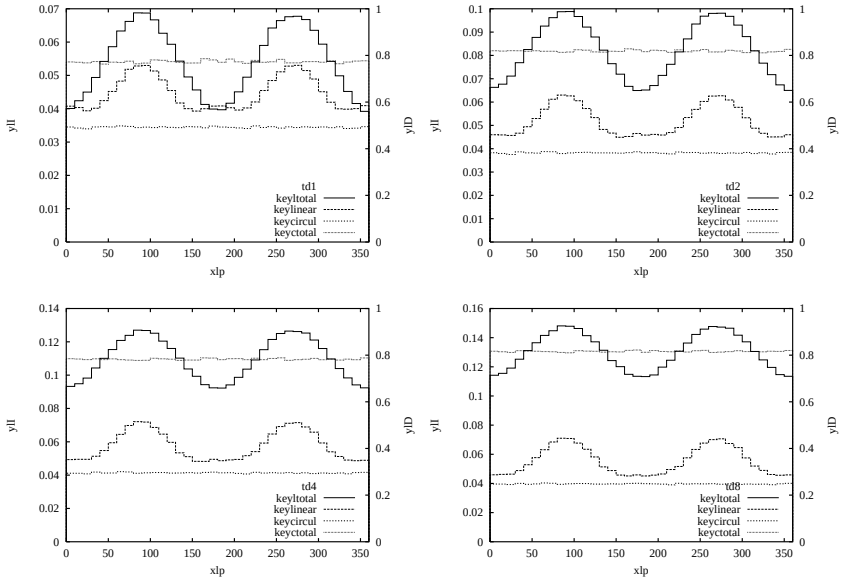

Fig. 15. Plots of backscattered intensity per unit solid angle against azimuthal angle at screen positions of $z = 1, 2, 4, 8$

situations, where the phase functions are taken to be heuristic, or the diagnostics have not been formulated in terms of experimental measurables.

The chief result is that a linear polarization state is better preserved than a circular state whatever gauge of measurement is used. This is seen both in transmission through the slab and in backscatter and is quantified in terms of the dimensionless 'degree of polarization', being a ratio of the absolute difference between orthogonal polarization states and their sum. This robust result stems from the form that the scattering phase functions adopt for different polarization states, as depicted in Fig. 3. For linear states, the phase function is greatest in the plane containing the direction of propagation of the ray and normal to the polarization vector, and possesses a significant cleft in the plane orthogonal to this. By comparison, the circular case has a more isotropic distribution, with the cleft being effectively filled in.

Unsurprisingly, multiple scattering causes the initially collimated beam to spread with depth into the medium and also in the backscattered direction. Close to the axis the degree of polarization is greatest because most of the light is either unscattered or has been scattered only once. Figure 11 shows the spread of backscattered light for slabs of increasing thickness, or equivalently, decreasing mean free path between scatterers. The curves depicting the degree of polarization are essentially independent of the depth of the medium, indicating that single scattering effects are dominant in backscatter. Allied to the spreading of the beam is the direction in which the rays

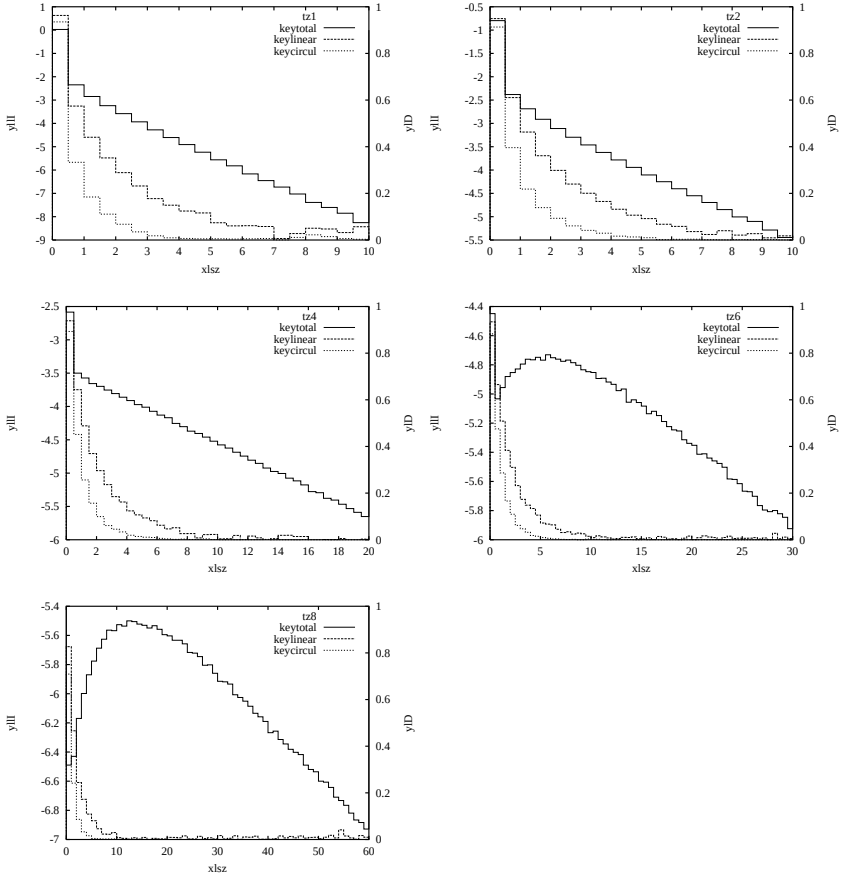

Fig. 16. The logarithm of transmitted intensity as a function of path-length traversed by a ray at reference depths of $z = 1, 2, 4, 6, 8$. Each horizontal scale has been offset by the depth of each measurement plane. The last graph has a bin width of 1 mean free path and furthermore its intensity has divided by two to ensure the same vertical scaling

are propagating when detected and this aspect will clearly impinge upon imaging considerations. The degree of polarization is weakly dependent on the polar angle for $\theta < 40°$, denoting the direction of the ray (as shown in Figs. 12 & 13) but the linear state is preserved better than the circular, a result that once again can be attributed to the form of the phase function (2) and the single scattering intensities (16–21). The invariance of the curves for backscattered light with increasing slab thickness (Fig. 13) reinforces the view that backscatter is dominated by single scattering effects from the medium. In transmission the direction of the rays are effectively randomized after propagating through eight mean free paths into the medium. The degree

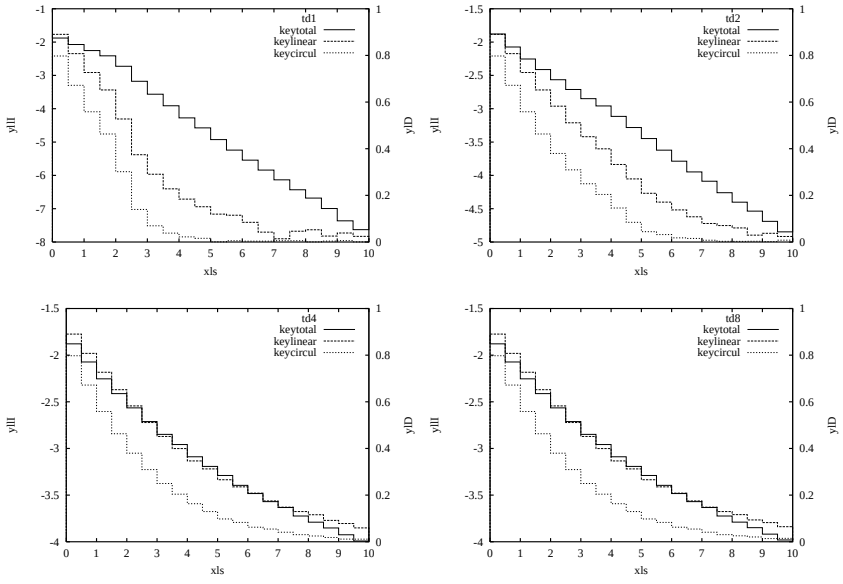

Fig. 17. Logarithm of the backscattered intensity as a function of path-length for slabs of thickness $z = 1, 2, 4, 8$

of polarization in either state is shown as a function of azimuthal angle in Figs. 14 & 15 and these illustrate the isotropy/anisotropy between circular and linear polarization which ties in with the results of [7]. Once again the linear state is essentially randomized on propagating about eight mean free paths into the medium.

A useful diagnostic of the model is the path length taken by each ray. This can be interpreted as the time of flight taken by a photon. Figures 16 & 17 show that for a given slab thickness there is a most likely path length for an ensemble of rays to follow. The probability for the occurrence of unscattered 'ballistic' rays, which are observed for thin slabs, naturally decreases with increasing slab thickness.

Acknowledgments

The authors would like to thank Drs. G. Lewis and D. Jordan for useful discussions with regard to this paper. This work was funded by Defence Evaluation and Research Agency, Malvern, UK.

A Appendix: Scattering Geometry and Derivation of the Phase Function

This appendix gives further details of the scattering geometry and representation of the polarization state used in the simulations. A ray having initial direction $\mathbf{d}$ and polarization $\mathbf{S}$ is scattered by angle Θ and rotated by Φ to a new direction $\mathbf{d}'$ and new polarization $\mathbf{S}'$. Figure 2 illustrates the ray directions where the arcs are parts of great circles on a unit sphere so the spherical polar coordinates of $\mathbf{d}$, angles (θ, ϕ) are arc lengths $z\mathrm{P}$ and $x\mathrm{Q}$. For $\mathbf{d}'$ (θ', ϕ') are the lengths $z\mathrm{P}'$ and $x\mathrm{Q}'$. These angles are related by

$$\mathbf{d} \cdot \mathbf{d}' = \cos\Theta \tag{8}$$

and

$$\mathbf{d}' = \mathbf{R}_z(\phi)\mathbf{R}_y(\theta)\mathbf{R}_z(\Phi)\mathbf{R}_y(\Theta)\mathbf{R}_y(-\theta)\mathbf{R}_z(-\phi)\mathbf{d} \tag{9}$$

where $\mathbf{R}_y$ and $\mathbf{R}_z$ are rotation matrices about the y and z axes respectively.

Linearly polarized light can be resolved into two orthogonal components in a plane perpendicular to its direction of propagation. To do so requires a reference polarization axis relative to which these components can be measured. A local coordinate frame is attached to each ray which is transformed whenever the ray changes direction. The reference axis is defined by the local $\hat{\theta}$ direction in the spherical polar representation of the ray's direction vector $\mathbf{d}$. This axis is also the line of intersection between the plane at P that is perpendicular to $\mathbf{d}$ and the plane containing both the z-axis and $\mathbf{d}$. In Fig. 2 the reference axis is the tangent to the great circle that passes through Pz. However if a ray travels in the z direction, the x-axis is used as the reference axis.

When a redefinition of the polarization reference axis takes place the components of the Stokes vector must also transform as

$$\mathbf{S} \to \mathbf{T}(\alpha)\mathbf{S} \tag{10}$$

where α is the angle of rotation with respect to the ray direction and $\mathbf{T}$ is given by (5). Note that the first and last components of $\mathbf{S}$ are invariant to rotations.

The Mueller matrix $\mathbf{M}$ describes how an optical device affects light represented by a Stokes vector:

$$\mathbf{S} \to \mathbf{MS}\,. \tag{11}$$

So for a scattering event $\mathbf{M}$ would describe the way the polarization transforms.

To keep the adopted polarization convention intact requires pre-rotating the reference axis, which lies along the arc $z\mathrm{P}$, to the scattering plane defined

by POP′. After scattering, a post-rotation is applied so that the reference axis lies on the arc $z\mathrm{P}'$, in keeping with the stated convention. Hence the Stokes vector must be transformed accordingly:

$$\mathbf{S}' = \mathbf{T}(-\alpha)\mathbf{M}(\Theta, \Phi, \theta, \phi)\mathbf{T}(\Phi)\mathbf{S} \tag{12}$$

where for spherical particles $\mathbf{M}$ is given by (3) and depends on Θ. From figure 2, the angle α is given by

$$\cos\alpha = \frac{\cos\theta - \cos\theta'\cos\Theta}{\sin\theta'\sin\Theta}\,. \tag{13}$$

The domain of α depends on the value of Φ in the following manner: $0 \leq \alpha \leq \pi$ for $0 \leq \Phi \leq \pi$ and $-\pi < \alpha < 0$ for $\pi \leq \Phi \leq 2\pi$. It is also important to note that there are several special cases that arise from using a spherical polar coordinate system. In these cases, (9), (12) & (13) can be singular and the transformed quantities must be calculated in an alternative manner. This particular detail is crucial to the implementation of the simulation as errors (such as dividing by zero) can otherwise occur. These singularities are due to the choice of coordinate system.

The phase function follows from (12). Generally the scattered intensity can be written in the form

$$I'(\mathbf{d}') \propto P(\Theta, \Phi, \mathbf{S}, \mathbf{d})I(\mathbf{d})\,. \tag{14}$$

The phase function is normalized according to the relation

$$\int_{\text{all angles}} \mathrm{d}\Omega\; P(\Theta, \Phi, \mathbf{S}, \mathbf{d}) = 1 \qquad \forall\ \mathbf{S} \text{ and } \mathbf{d}\,, \tag{15}$$

which determines the constant of proportionality in (14). For Rayleigh scatterers the phase function (2) does not depend on $\mathbf{d}$ because the scattering particle is assumed to be a sphere.

The state of a singly scattered ray is easily deduced from (4). When the light is linearly polarized, the total scattered intensity is

$$I = (1/2)\left[\mu^2 + 1 + \left(\mu^2 - 1\right)\cos 2\Phi\right]\,, \tag{16}$$

the co-polar intensity is

$$I_{\text{co}} = (1/4)\left[|\mu| + 1 + (|\mu| - 1)\cos 2\Phi\right]^2 \tag{17}$$

and cross-polar intensity is

$$I_{\text{cross}} = (1/4)\left(|\mu| - 1\right)^2 \sin^2 2\Phi\,. \tag{18}$$

For incident light that is circularly polarized the total intensity is

$$I = (1/2)\left(\mu^2 + 1\right)\,, \tag{19}$$

the right-circularly polarized intensity is

$$I_{\text{right}} = (1/4)\,(\mu + 1)^2 \tag{20}$$

and left circular intensity is

$$I_{\text{left}} = (1/4)\,(\mu - 1)^2\ . \tag{21}$$

The phase functions are plotted in Fig. 3, the intensities in each polarization are shown in Figs. 4 and 5.

References

1. S. Karp, R.M. Gagliardi, S.E. Moran & L.B. Stotts (1988) *Optical Channels*, Plenum Press, NY
2. S. Chandrasekhar (1960) *Radiative Transfer*, Dover Publications, NY
3. J.J. Duderstadt & W.R. Martin (1979) *Transport Theory*, John Wiley & Sons, NY
4. A. Ishimaru (1978) *Wave Propagation and Scattering in Random Media* Vol. 1 & 2, Academic Press, NY
5. S. Ito (1981) "Theory of beam light pulse propagation through thick clouds: effects of beamwidth and scatterers behind the light source on pulse broadening," *Appl. Opt.* **20**, 2706–15
6. K.M. Yoo & R.R. Alfano (1989) "Time resolved depolarization of multiple backscattered light from random media," *Phys. Lett. A* **142**, 531–5
7. R.L-T. Cheung & A. Ishimaru (1982) "Transmission, backscattering, and depolarization of waves in randomly distributed spherical particle," *Appl. Opt.* **21**, 3792–3798
8. M.J. Stephen & G. Cwilich (1986) "Rayleigh scattering and weak localization: Effects of polarization," *Phys. Rev.* B **34**, 7564–72
9. D. Eliyahu, M. Rosenbluh & I. Freund (1993) "Angular intensity and polarization dependence of diffuse transmission through random media," *J. Opt. Soc. Am.* A **10**, 477–91
10. F.C. MacKintosh & S. John (1989) "Diffusing-wave spectroscopy and multiple scattering of light in correlated random media," *Phys. Rev.* B **40**, 2383–406 ; K.J. Peters (1992) " Coherent-backscatter effect: A vector formulation accounting for polarization and absorption effects and small or large scatterers," *Phys. Rev.* B **46**, 801–12 ; F.C. MacKintosh, J.X. Zhu, D.J. Pine & D.A. Weitz (1989) "Polarization memory of multiply scattered light," *Phys. Rev.* B **40**, 9342–5
11. D. Bicout & C. Brosseau (1992) "Multiply scattered waves through a spatially random medium: entropy production and depolarization," *J. Phys. I France* **2**, 2047–63
12. G.N. Plass & G.W. Kattawar (1992) "Monte Carlo calculations of light scattering from clouds," *Appl. Opt.* **7**, 415–9
13. G.N. Plass & G.W. Kattawar (1973) "Reflection of light pulses from clouds," *Appl. Opt.* **10**, 2304–10 (1971); E.A. Bucher, "Computer simulation of light pulse propagation for communication through thick clouds," *Appl. Opt.* **12**, 2391–400

14. B. Maheu, J.-P. Briton & G. Gouesbet (1989) "Four-flux model and a Monte Carlo code: comparisons between two simple, complementary tools for multiple scattering calculations," *Appl. Opt.* **28**, 22–4 ; J.-P. Briton, B. Maheu, G. Gréhan & G. Gouesbet (1992) "Monte Carlo simulation of multiple scattering in arbitrary 3-D geometry," *Part. Part. Syst. Charact.* **9**, 52–8
15. P. Bruscaglioni, P. Donelli, A. Ismaelli & G. Zaccanti (1991) "A numerical procedure for calculating the effect of a turbid medium on the MTF of an optical system," *J. Mod. Optics* **38**, 129–42 ; P. Donelli, P. Bruscaglioni, A. Ismaelli & G. Zaccanti (1991) "Experimental validation of a Monte Carlo procedure for the evaluation of the effect of a turbid medium on the point spread function of an optical system," *J. Mod. Optics* **38**, 2189–201
16. G.W. Kattawar & G.N. Plass (1968) "Radiance and polarization of multiple scattered light from haze and clouds," *Appl. Opt.* **7**, 1519–27 ; G.W. Kattawar & G.N. Plass (1972) "Degree and direction of polarization of multiple scattered light. 1: Homogeneous cloud layers," *Appl. Opt.* **11**, 2851–65
17. T. Aruga & T. Igarashi (1981) "Narrow beam light transfer in small particles: image blurring and depolarization," *Appl. Opt.* **20**, 2698–705; corrected in T. Aruga & T. Igarashi (1981) *Appl. Opt.* **20**, 3831
18. J.M. Schmitt, A.H. Gandjbakhche & R.F. Bonner (1992) "Use of polarized light to discriminate short-path photons in a mulitply scattering medium," *Appl. Opt.* **31**, 6535–46
19. P. Bruscaglioni, G. Zaccanti & Q. Wei (1993) "Transmission of a pulsed polarized light beam through thick turbid media: numerical results," *Appl. Opt.* **32**, 6142–50
20. D. Bicout, C. Brosseau, A.S. Martinez & J.M. Schmitt (1994) "Depolarization of multiply scattered waves by spherical diffusers: Influence of the size parameter," *Phys. Rev.* E **49**, 1767–70 ; A.S. Martinez & R. Maynard (1994) "Faraday effect and multiple scattering of light," *Phys. Rev.* B **50**, 3714–32
21. O. Fischer, Th. Henning & H.W. Yorke (1994) "Simulation of polarization maps. I. Protostellar envelopes," *Astronomy and Astrophysics* **284**, 187–209
22. W.J. Henney & D.J. Axon (1995) "Polarization profiles of scattered emission lines. III. Effects of multiple scattering and non-Rayleigh phase functions," *Astrophys. J.* **454**, 233–53
23. S. Bianchi, A. Ferrara & C. Giovanardi (1996) "Monte Carlo simulations of dusty spiral galaxies: Extinction and polarization properties," *Astrophys. J.* **465**, 127–44
24. H.C. van de Hulst (1981) *Light Scattering by Small Particles*, Dover Publications, NY
25. L.C. Henyey & J.L. Greenstein (1941) "Diffuse radiation in the galaxy," *Astrophys. J.* **93**, 70-83
26. E.D. Cashwell & C.J. Everett (1959) *Monte Carlo Method for random walk problems*, Pergamon Press, NY
27. P. Bratley, B.L. Fox & L.E. Schrage (1983) *A Guide to Simulation*, Springer-Verlag, NY
28. B. Jansson (1966) *Random Number Generators*, Victor Pettersons, Stockholm
29. W.H. Press, S.A. Teukolsky, W.T. Vetterling & B.P. Flannery (1992) *Numerical Recipes in C*, 2nd Ed. CUP
30. A.P. Bates, K.I. Hopcraft & E. Jakeman (1997) "Particle shape determination from polarization fluctuations of scattered radiation," *J. Opt. Soc. Am.* A **14**, 3372–8